# Static and dynamical properties of frustrated two-dimensional square quantum Heisenberg antiferromagnets

Saori Kurata,* Chigusa Sasaki, and Kazuko Kawasaki
*Department of Physics, Nara Women's University, Nara 630-8506, Japan*
(Received 10 January 2000; revised manuscript received 28 March 2000; published 18 December 2000)

Two-dimensional square quantum Heisenberg antiferromagnets with competing interactions up to third neighbors ($J_1$-$J_2$-$J_3$ model) are investigated by using the high-temperature series expansion method. From the analyses of the wave-vector-dependent susceptibility $\chi(\boldsymbol{k})$, we find four kinds of the stable paramagnetic phases depending on the coupling constants, i.e., *Néel*, *collinear*, and two helical paramagnetic phases, $H_1$ and $H_2$. They are characterized by the critical wave vector $\boldsymbol{k}_A^c$ ($A=N$, $C$, $H_1$, or $H_2$), at which the functions $\chi(\boldsymbol{k})$ show the maximum value. Except around the $H_1$-$H_2$ phase boundary, they are destabilized and show the intermediate phases in the neighborhood of the phase boundaries, where the relevant critical wave vector $\boldsymbol{k}_A^c$ is not specified uniquely. The analogy between the paramagnetic phase diagram obtained here and the ordered ones derived by the simple spin wave theory suggests the possibility of the spin liquid state in the intermediate phase at $T=0$. The first-order transition occurs between $H_1$ and $H_2$ phases, so the intermediate phase is not seen there. The dynamical spectrum function $F(\boldsymbol{k},\omega)$ is calculated in the form of Mori's continued fraction with the frequency moments. The dynamical aspects for the stable paramagnetic phases are also characterized by the critical wave vector $\boldsymbol{k}_A^c$. While the side peak or shoulder shape appears in $F(\boldsymbol{k}_A^c,\omega)$ at $T=\infty$, the line shape becomes considerably narrow when decreasing the temperature at $\boldsymbol{k}_A^c$. These behaviors are attributed to the spin flip-flop motion for the former case, and the quasicollective motion for the latter one. In the intermediate phase, at $T=\infty$ the line shape undergoes slow change versus the wave vector $\boldsymbol{k}$ except for the drastic narrowing around $\boldsymbol{k}\simeq 0$, due to the absence of the unique critical wave vector. It is found that the high-temperature dynamical aspect keeps there, even though the temperature is decreased, due to the frustration effect.

DOI: 10.1103/PhysRevB.63.024412 PACS number(s): 75.10.Jm, 75.25.+z, 75.40.Gb, 75.50.Ee

## I. INTRODUCTION

Frustration in magnetic systems is well known to be responsible for a number of curious phenomena. One of the more interesting features is the possible existence of the spin liquid, in which long-range order at absolute zero temperature is destroyed when the frustration effect is significant. For two-dimensional (2D) square antiferromagnetic Heisenberg magnets composed of first- and second-neighbor interactions ($J_1$-$J_2$ model), there are two contradictory predictions[1] regarding the spin liquid state: One is that there exists a disordered phase under a certain value of the second-neighbor interaction;[1,2] and the other is that the classical-ordered phases are always stable against the frustration and quantum fluctuation, so the spin-disordered state may not appear but the first-order transition does.[3] In addition to these predictions, it has recently been argued[4] that the spin liquid state could survive in the $J_1$-$J_2$-$J_3$ model with proper frustration parameters, where the spin system consists of up to third-neighbor interactions. The phase diagram is obtained using spin-wave theory by Moreo *et al.*,[5] and four kinds of ordered phases are clarified. In addition to it, the disordered regions are suggested in the vicinity of phase boundary.

Besides, the recent discovery of the high-temperature superconductor,[6] such as 2D antiferromagnets in $La_{2-x}Sr_xCuO_4$ and $YBa_2Cu_3O_{7-x}$, calls ones interest to the problem of the disordered frustrated spin systems,[7] because it is supposed that the frustration effect is related to the doping effect, which is an important issue for the mechanism of the high-$T_c$ superconductor. While the Hamiltonian relevant to it is known as the $t$-$J$ model with hole doping, recently the $J_1$-$J_2$ model was proposed by Doniach *et al.*,[8] in a semiphenomenlogical fashion, to capture the physics of frustration induced to the system by hole doping. Moreo *et al.* also[5] conjectured that a relation may exist between the $t$-$J$ model with hole doping and the $J_1$-$J_2$-$J_3$ model for the particular case of $J_3=J_2/2$, with $J_1=1$.

The aim of this paper is to investigate the frustration effect on dynamic properties as well as static ones, especially in the critical temperature region. We consider a 2D square frustrated quantum antiferromagnet Heisenberg ($S=1/2$), which contains up to third-neighbor couplings ($J_1$-$J_2$-$J_3$ model). The Hamiltonian is written by

$$\mathcal{H}=J_1\sum_{\langle ij\rangle}\boldsymbol{S}_i\cdot\boldsymbol{S}_j+J_2\sum_{\langle il\rangle}\boldsymbol{S}_i\cdot\boldsymbol{S}_l+J_3\sum_{\langle im\rangle}\boldsymbol{S}_i\cdot\boldsymbol{S}_m, \qquad (1)$$

where $J_1$, $J_2$, and $J_3$ are the first-, second-, and third-nearest-neighbor coupling constants, respectively, and all of $J_i$ ($i=1,2,3$) are considered to be positive. The notations $\langle ij\rangle$, $\langle il\rangle$, and $\langle im\rangle$ denote the first-, second-, and third-$nn$ pairs of spins, respectively.

The wave vector dependence of the static susceptibility $\chi(\boldsymbol{k})$ helps us in understanding various critical phenomena.[9] The features of the local order developed at the critical regime can be studied by the analyses of the temperature and the wave-vector dependences of the function. Moreover, it leads us to determine the magnetic configuration of long-range order below the critical point, because it is characterized by the critical wave vector $\boldsymbol{k}_c$, at which the function

 

$\chi(\boldsymbol{k})$ shows its maximum value in the paramagnetic phase. As for dynamics, the dynamical spectrum function $F(\boldsymbol{k},\omega)$ gives us significant information because it is directly proportional to the inelastic diffuse thermal neutron scattering cross section.[9] Therefore, we can get physical interpretation for the theoretical results by referring to the related experimental data. Under these situations, the studies of $\chi(\boldsymbol{k})$ and $F(\boldsymbol{k},\omega)$ with arbitrary $\boldsymbol{k}$ and $\omega$ are expected to shed light on the problem of the frustrated spin systems.

We calculate these functions by the high-temperature series expansion method, i.e., they are expanded in powers of the inverse temperature $\Theta(\equiv J_1/k_BT)$. We carry out the function $\chi(\boldsymbol{k})$ up to seventh order of $\Theta$. Using the $m$th frequency moments of $F(\boldsymbol{k},\omega)$, which are calculated up to $\Theta^6$, $\Theta^5$, $\Theta^3$, and $\Theta$ for $m=0$, 2, 4, and 6, respectively, the function $F(\boldsymbol{k},\omega)$ is constructed through the form of Mori's continued fraction.[10]

The high-temperature series expansion method is a useful tool to investigate the frustration effect in disordered systems for the following reasons. First, by using this method one can study various magnetic properties without thinking about the sublattice structure of ordered states in advance. Second, it includes all nonlinear effects of thermal fluctuation at the corresponding order of expansion, which is ignored in the mean-field theory. So far, we employed this method to study several complex spin systems, such as randomly diluted Heisenberg paramagnets on a Bravais lattice with a quenched-site or exchange-bond dilution,[11] and with a couple of competing interactions.[12] These theories give us a proper understanding of the experimental results for various quantities, i.e., the transition temperature, the magnetic concentration dependence in the specific heat, susceptibility, etc. Many other works related to this method have been reviewed by Rushbrooke, Baker, and Wood.[13]

This paper is organized as follows: In Sec. II, the expression of the high-temperature series expansion is presented for the static susceptibility $\chi(\boldsymbol{k})$, and the procedure for estimation of the quantities is explained. Especially, we are concerned with the static properties for the 2D square quantum $J_1$-$J_2$-$J_3$ Heisenberg antiferromagnets by analyses of the wave vector and the temperature dependence for $\chi(\boldsymbol{k})$. The dynamical spectrum function $F(\boldsymbol{k},\omega)$ is calculated in the form of Mori's continued fraction in Sec. III. We discuss some peculiarities in spin dynamics of the present $J_1$-$J_2$-$J_3$ model by the studies of $J_i$ $(i=1,2,3)$ dependence of $F(\boldsymbol{k},\omega)$. This paper ends with a summary in Sec. IV.

## II. THE STATIC SUSCEPTIBILITY

We analyze the wave-vector-dependent susceptibility $\chi^{zz}(\boldsymbol{k})$ in terms of the high-temperature series expansion. This function is defined as

$$\chi^{zz}(\boldsymbol{k})=(g\mu_B)^2\beta\sum_{\boldsymbol{lj}}\exp\{i\boldsymbol{k}\cdot(\boldsymbol{l}-\boldsymbol{j})\}\int_0^\beta d\lambda\langle S_{\boldsymbol{l}}^z S_{\boldsymbol{j}}^z(i\hbar\lambda)\rangle, \tag{2}$$

where $\beta$ is defined by $1/k_BT$, $\mu_B$ is the Bohr magneton, and $g$ the gyromagnetic ratio. Because of the spatial isotropy of the system in the paramagnetic phase, the superscript $z$ is omitted hereafter. The time dependence of the operator $B(t)$ is in the Heisenberg representation, i.e.,

$$B(t)=\exp(i\mathcal{H}t)B(0)\exp(-i\mathcal{H}t), \tag{3}$$

and the angular brackets denote a canonical thermal average at Kelvin temperature $T$, i.e.,

$$\langle A\rangle=\frac{\mathrm{Tr}[\exp(-\beta\mathcal{H})A]}{\mathrm{Tr}[\exp(-\beta\mathcal{H})]}. \tag{4}$$

In the high-temperature series expansion expression, $\chi(\boldsymbol{k})$ is written as

$$\chi(\boldsymbol{k})=[(g\mu_B)^2/J_1]\sum_{n=1}^{\infty}X_n(j_2,j_3;\boldsymbol{k})\Theta^{-n}, \tag{5}$$

where $j_i$ and $\Theta$ are defined as $J_i/J_1$ $(i=2,3)$, and a dimensionless reduced temperature $k_BT/J_1$, respectively. The calculated coefficients $X_n(j_2,j_3;\boldsymbol{k})$ are given[14] at symmetry point $\Gamma$, $X$, and $M$, for $1\leqslant n\leqslant 7$ by putting $S=1/2$.

Present treatment for the series expansion corresponds to the linked-cluster expansion method. It contains up to seven-bond clusters. To count bond clusters, we have to take care of the relative position of two sites $\boldsymbol{l}$ and $\boldsymbol{j}$. For example, there are two kinds of one-bond cluster, depending on whether sites $\boldsymbol{l}$ and $\boldsymbol{j}$ are the same position or not, i.e., $\delta_{\boldsymbol{lj}}$ or $1-\delta_{\boldsymbol{lj}}$. As a result, the numbers $n(m)$ for $m$-bond cluster are $n(1)=2$, $n(2)=4$, $n(3)=12$, $n(4)=24$, $n(5)=54$, $n(6)=69$, and $n(7)=83$. When we estimate the quantity of $\chi(\boldsymbol{k})$, from this method, we always check the convergence of the series by $1/n$ plotting. Namely, we draw $\chi^{[n]}(\boldsymbol{k})$, which contains terms, up to the $n$th order, against $1/n$. Afterward, $\chi(\boldsymbol{k})$ is extrapolated from the mean value of $\chi^{[6]}(\boldsymbol{k})$ and $\chi^{[7]}(\boldsymbol{k})$, unless $\chi^{[n]}(\boldsymbol{k})$ shows oscillatory behavior with divergent amplitude as $1/n\to 0$.

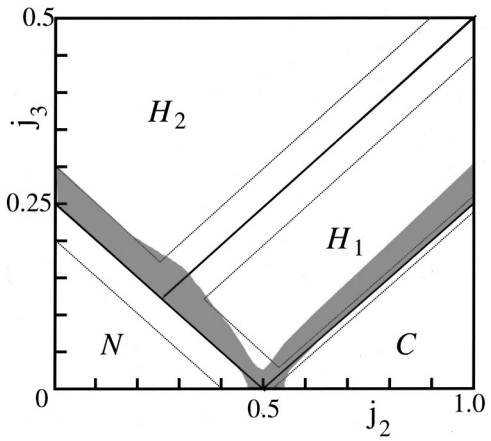


FIG. 1. Zero-temperature phase diagram for $S=1/2$ in the $j_2$-$j_3$ parameter space. The solid lines denote the phase boundaries determined by the simple spin-wave theory (Ref. 5). The existence of the spin-liquid phase is suggested in the region surrounded by dotted lines. As will be shown in Sec. II, the present theory indicates the intermediate phase in the shaded areas, which are called domains.

Before describing the calculated results, the zero-temperature phase diagram for $S=1/2$ determined by the linear spin-wave theory[5] is presented in Fig. 1. Depending on parameters $j_2$ and $j_3$, four distinct phases are seen: *Néel*, *collinear*, and two helical configurations $H_1$ and $H_2$. For convenience, we refer to them hereafter as $N$, $C$, $H_1$, and $H_2$ phases, respectively. They are characterized by the wave vector

$$\boldsymbol{k}_N^c=(\pi,\pi), \tag{6a}$$

$$\boldsymbol{k}_C^c=(0,\pi) \quad \text{or} \quad (\pi,0), \tag{6b}$$

$$\boldsymbol{k}_{H_1}^c=\left(\cos^{-1}\left[\frac{(2j_2-1)}{4j_3}\right],\pi\right) \quad \text{or} \quad \left(\pi,\cos^{-1}\left[\frac{(2j_2-1)}{4j_3}\right]\right), \tag{6c}$$

$$\boldsymbol{k}_{H_2}^c=\left(\cos^{-1}\left[\frac{-1}{(2j_2+4j_3)}\right],\quad \cos^{-1}\left[\frac{-1}{(2j_2+4j_3)}\right]\right), \tag{6d}$$

respectively. In Fig. 1, the continuous lines denote the boundaries between two different phases in the classical limit $S=\infty$, and the region surrounded by dotted lines indicates something like the spin liquid state for $S=1/2$ in a sense of disordered phase in spite of the ground state.

As is well known, 2D isotropic Heisenberg systems have no finite transition point.[15] Then it is convenient to study the various features of $\chi(\boldsymbol{k})$ with different coupling constants $j_i$'s on the basis of the reduced temperature $\tilde{T}(\equiv T/T_{MC})$, where $T_{MC}$ is the transition temperature determined by the mean-field theory, i.e.,

$$3k_BT_{MC}/2S(S+1)J_1 = \begin{cases} (1-j_2-j_3)/3 & \text{for } N \text{ phase} \quad (7a)\\ (j_2-j_3)/3 & \text{for } C \text{ phase} \quad (7b)\\ [-\cos k_x^c+1+2j_2\cos k_x^c-j_3(\cos 2k_x^c+1)]/6 & \text{for } H_1 \text{ phase} \quad (7c)\\ [-\cos k_x^c-\cos k_y^c-2j_2\cos k_x^c\cos k_y^c-j_3(\cos 2k_x^c+\cos 2k_y^c)]/6 & \text{for } H_2 \text{ phase.} \quad (7d) \end{cases}$$

In Figs. 2(a)–2(d), the susceptibility $\chi(\boldsymbol{k})$, which is normalized by the value at the high-temperature limit, is illustrated on the $(k_x$-$k_y)$ plane at $\tilde{T}=3.0$ for four cases with parameters $J_1=1.0$ where $(j_2,j_3)$ is (0,0), (2.0,0), (1.0,0.375), and (0,1.0), respectively. The corresponding contour plots are also given on the right-hand side. As is shown in Fig. 1, they are expected to be typically ordered states named $N$, $C$, $H_1$, and $H_2$ phases at $T=0$, respectively. We can find in Fig. 2 that each $\chi(\boldsymbol{k})$ exhibits a broad maximum centralized at the proper critical wave vector $\boldsymbol{k}_A^c$ ($A=N$, $C$, $H_1$, or $H_2$), determined by Eqs. (6a)–(6d), whereas they have no $\boldsymbol{k}$ dependence at $T=\infty$. We call these paramagnetic phases, the $A$ paramagnetic phase, if $\chi(\boldsymbol{k})$ shows a broad maximum at $\boldsymbol{k}_A^c$. It is found that the position of the critical wave vector $\boldsymbol{k}_A^c$ is unchanged at decreased temperature, but the shape of $\chi(\boldsymbol{k})$ becomes gradually sharpened. Therefore, the pattern of the local order developed at the critical temperature is characterized by $\boldsymbol{k}_A^c$, and the ordered state seems to be inherited from it. In this sense, the analysis of $\chi(\boldsymbol{k})$ calculated in terms of the high-temperature series expansion allows us to study the critical behavior for general cases with arbitrary parameters $(j_2,j_3)$, and to discuss whether the spin liquid state exists or not in the present $J_1$-$J_2$-$J_3$ model, and what kind of aspect results if it exists. For convenience, we use the reduced wave vector $\bar{\boldsymbol{k}}$ defined by $\boldsymbol{k}/\pi$ in the following discussions.

Since the possibility of the spin liquid state is suggested[5] around $j_3\cong j_2/2$, where $j_2>0.25$ and $j_3>0.125$, which is a border line between $H_1$ and $H_2$ phases, and $j_3=(1-2j_2)/4$, where $j_2<0.5$, which is the boundary between $N$ and $H_1$ or $H_2$ phases (see Fig. 1), let us observe $\chi(\boldsymbol{k})$ along two lines $j_2=0.5$ and $j_3=(1-2j_2)/4$, where $j_2<0.5$. By fixing the parameter as $j_2=0.5$, $\chi(\boldsymbol{k})$ is displayed in Fig. 3 at $\tilde{T}=3.0$ for (a) $j_3=0$, (b) 0.125, (c) 0.25, and (d) 0.5, respectively. Four distinguishable peaks are seen in $\chi(\boldsymbol{k})$ at $\bar{\boldsymbol{k}}_{H_1}^c=(1.0\pm0.5,1.0)$ and $(1.0,1.0\pm0.5)$ in (b), and at $\bar{\boldsymbol{k}}_{H_2}^c\cong(1.0\pm0.4,1.0\pm0.4)$ in (d). The former indicates the $H_1$ paramagnetic phase, and the latter indicates the $H_2$-type phase. For the rest, however, we cannot recognize the specific peak position of $\chi(\boldsymbol{k})$; instead, $\chi(\boldsymbol{k})$ shows a broad maximum along the lines of $\bar{k}_x=1.0$ and $\bar{k}_y=1.0$ in (a), which is the $N$-$H_1$-$C$ triple point, and along a ring $(\bar{k}_x^2+\bar{k}_y^2)\cong(0.5)^2$ in (c), which corresponds to the $H_1$-$H_2$ phase boundary. In Fig. 4, $\chi(\boldsymbol{k})$ is plotted along another line, $j_3=(1-2j_2)/4$ at $\tilde{T}=2.5$ for the parameters $(j_2,j_3)$, which are (a) (0.1,0.2), (b) (0.25,0.125), and (c) (0.4,0.05), respectively. Each case corresponds to the $N$-$H_2$ boundary, the $N$-$H_1$-$H_2$ triple point, and the boundary between $N$ and $H_1$ phases, respectively. For each case, $\chi(\boldsymbol{k})$ displays its maximum over a certain range on the $(k_x$-$k_y)$ plane. In addition to the above cases, $\chi(\boldsymbol{k})$ is shown for $(j_2,j_3)=(0.75,0.125)$ in Fig. 4(d) at $\tilde{T}=3.0$, which corresponds to the $C$-$H_1$ phase boundary. From these results, one can find a certain spreading domain on the $(k_x$-$k_y)$ plane at the phase boundary, over which $\chi(\boldsymbol{k})$ remains constant with its maximum value, in contrast to the fact that typical $N$, $C$, $H_1$, and $H_2$ paramagnetic phases have their own specified

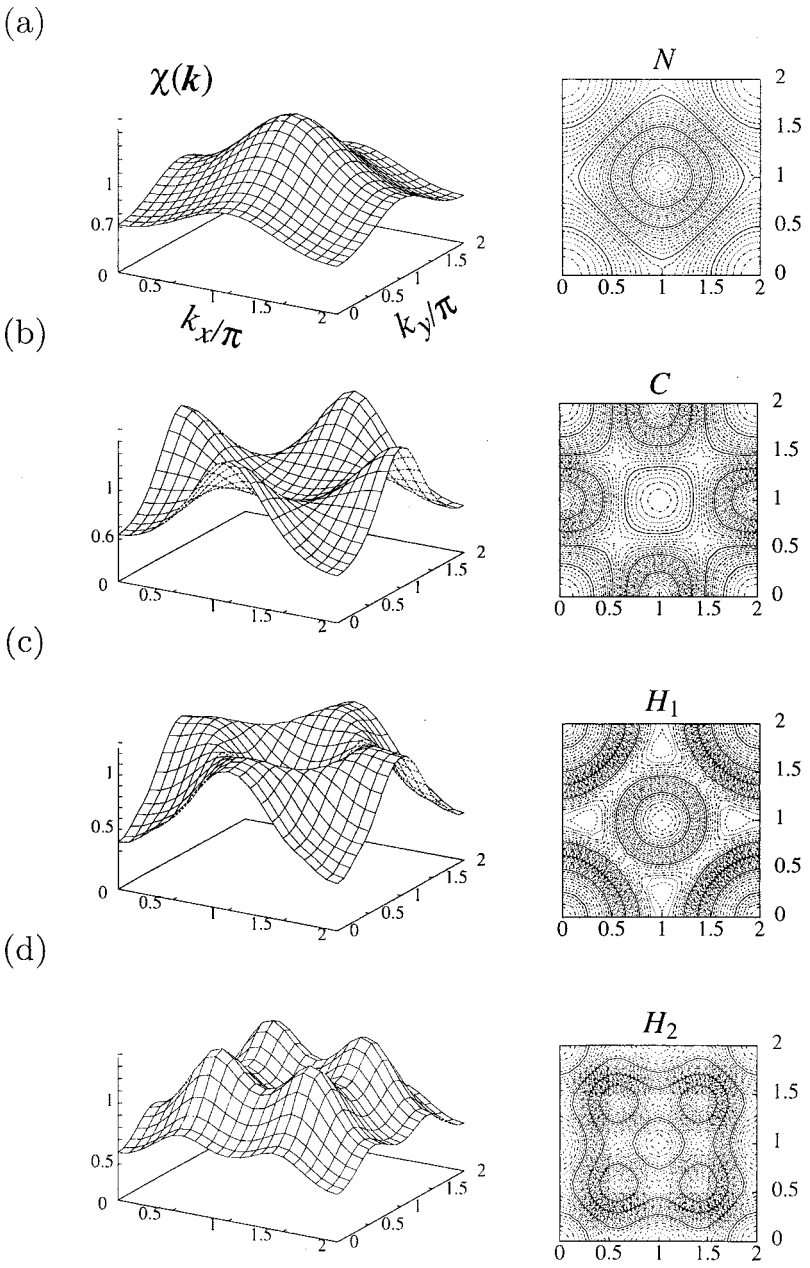


FIG. 2. The wave-vector-dependent susceptibility $\chi(\boldsymbol{k})$ for $S=1/2$ is illustrated for stable paramagnetic phases on the $(k_x$-$k_y)$ plane at $\tilde{T}=3.0$. The figures are normalized at $T=\infty$: (a) $N$ paramagnetic phase, with $j_2=j_3=0$; (b) $C$ paramagnetic phase with $j_2=2.0$ and $j_3=0$; (c) $H_1$ paramagnetic phase, with $j_2=1.0$ and $j_3=0.375$; and (d) $H_2$ paramagnetic phase with $j_2=0$ and $j_3=1.0$. The relevant contour map is presented on the right-hand side.

peak positions in $\chi(\boldsymbol{k})$. We find that the domain varies in form depending on the parameters $j_2$ and $j_3$. From their shapes, we refer to these domains appearing in Figs. 3(a) and 3(c) as ''cross'' and ''ring,'' respectively. Other domains in Figs. 4(a)–4(d) are also referred to as ''square,'' ''disk,'' ''diamond,'' and ''rectangular,'' respectively.

In Fig. 5 the temperature dependence of $\chi(\boldsymbol{k})$ is plotted along the $X$-$M$ direction for cases bring the following domains: in (a) cross, with $(j_2=0.5, j_3=0)$; (b) ring with (0.5,0.25), (c) disk with (0.25,0.15), and (d) rectangular with (0.75,0.125). Although the temperature is decreased, they show no definite unique critical wave vector but display curious wave-vector dependence. In Fig. 5(a), $\chi(\boldsymbol{k})$ heaps up so slightly centering around the $M$ point in the $X$-$M$ direction at $\tilde{T}=1.5$ that the difference between the maximum and the minimum value is less than 7%, whereas it presents a peak around $M$ in the $\Gamma$-$M$ direction, as shown in the inset. Figure 5(b) presents two distinguishable peaks near points of $(1.0 \pm 0.47, 1.0)$. However, they are not characteristic modes specifying the ordering type, but they express two sections of ring [see Fig. 3(c)]. The wave-vector-independent parts are seen in $\chi(\boldsymbol{k})$ around the $M$ point in Fig. 5(c) and the $X$ point in Fig. 5(d), due to the existence of the domain structure. These situations are confirmed when we plot the wave-vector dependence of the ground-state energy $E(\boldsymbol{k})$ determined by the spin-wave theory.[16] In that case, the critical wave vector $\boldsymbol{k}_A^c$ is determined by minimizing $E(\boldsymbol{k})$.

So far, we have been concerned with the feature of $\chi(\boldsymbol{k})$ just on the phase boundary; now let us pay our attention to it in the vicinity of the phase boundary. To do so, it is instructive to trace the peak position of $\chi(\boldsymbol{k})$, denoted by $\boldsymbol{k}_A^p$, with the variation of $j_i$ $(i=2,3)$. In Fig. 6, $\boldsymbol{k}_A^p$ is plotted for its $x$

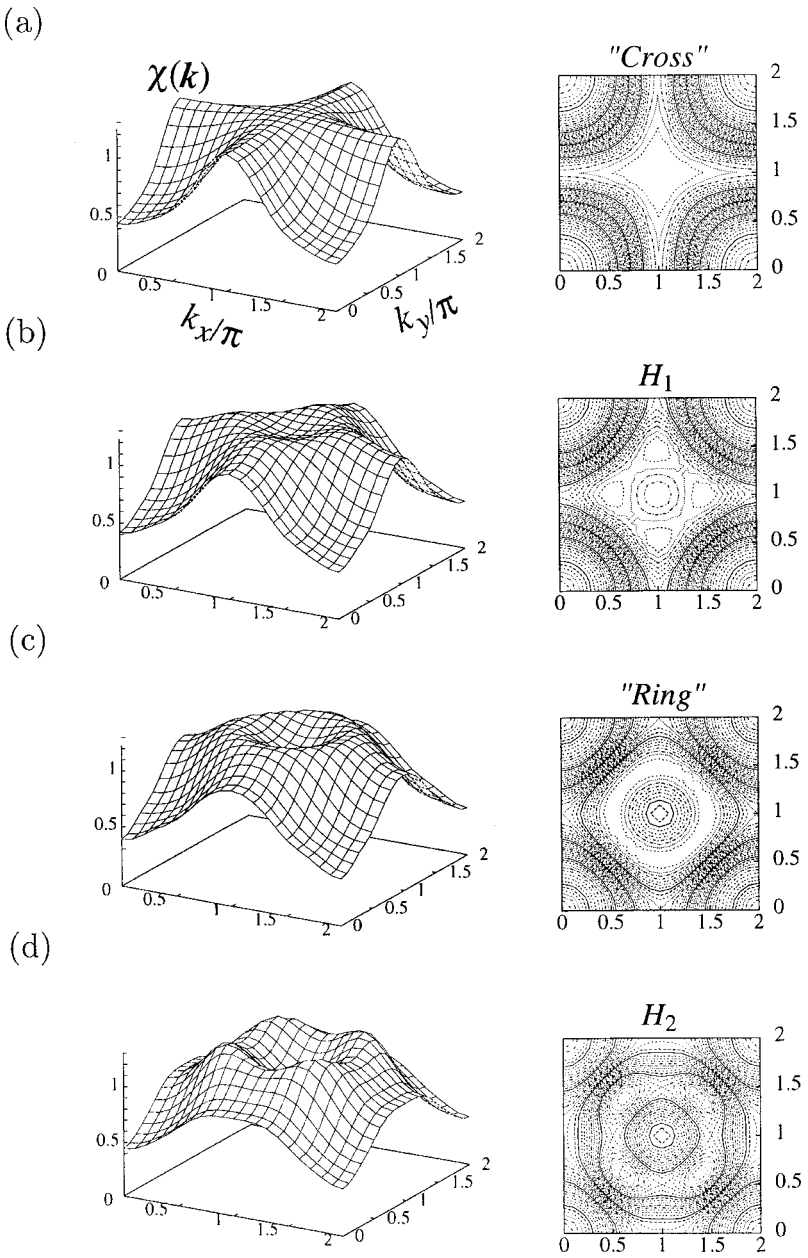


FIG. 3. The susceptibility $\chi(\boldsymbol{k})$ is plotted at $\tilde{T}=3.0$ along a line of $j_2=0.5$, with (a) $j_3=0$, (b) 0.125, (c) 0.25, and (d) 0.5, respectively. The relevant contour map is presented on the right-hand side.

component $(\boldsymbol{k}_A^p)_x$ versus various values of $j_3$ at $\tilde{T}=1.5$, (a) for $j_2=0.5$ and (b) for 0.75, respectively. As for the $j_2$ dependence, it is shown in Fig. 7 for (a) $j_3=0.125$ and (b) $j_3=0.2$, respectively. To examine the quantum effect, the corresponding classical values (with $S=\infty$) are displayed. For reference, $(\boldsymbol{k}_A^c)_x$ is also drawn. The phase limits determined by the spin-wave theory[5] are indicated by the arrows.

From these figures, we find the following facts.

(1) In the classical case, $(\boldsymbol{k}_A^p)_x$ coincides with $(\boldsymbol{k}_A^c)_x$ on the whole except in the shaded area; however, non-negligible discrepancies between them are seen in the quantal case, i.e., it deviates from the classical ones toward the *M* point as long as $j_2$ and/or $j_3$ are smaller than 0.5. This means that the quantal case is influenced by the *Néel* mode more efficiently.

(2) The $j_i$ $(i=2,3)$ dependence of $(\boldsymbol{k}_A^c)_x$ is classified into two types: one changes discontinuously at the phase boundary, while the other varies continuously, but abruptly, there. The former case occurs at the $H_1$-$H_2$ phase boundary. The peak position of $\chi(\boldsymbol{k})$ also jumps from $\boldsymbol{k}_{H_1}^p$ to $\boldsymbol{k}_{H_2}^p$, or vice versa. If the parameters $j_i$'s depart from the boundary point a little, it behaves like the stable $H_1$ or $H_2$ paramagnetic phase at once. Then this is considered as the first-order phase transition. Just at the phase boundary, the associated two characteristic modes $\boldsymbol{k}_{H_1}^c$ and $\boldsymbol{k}_{H_2}^c$ may coexist and stand on a circle $\overline{k_x^2}+\overline{k_y^2}\cong(0.5)^2$ for the considered case with $j_2=0.5$ and $j_3=0.25$. Consequently, the formation of the ring shape domain is acceptable on the $(k_x$-$k_y)$ plane. The latter case takes place at the $N$-$H_1$-$H_2$ triple point, and at the $H_1$-$C$, $N$-$H_1$, and $N$-$H_2$ phase boundaries. It is noteworthy that the domain structures come out in the vicinity of every phase boundary between the commensurate and incommensurate paramagnetic phases (see the shaded areas in Figs. 6 and 7). Since the critical wave vector $\boldsymbol{k}_{H_1}^c$ (and/or $\boldsymbol{k}_{H_2}^c$) in the incom-

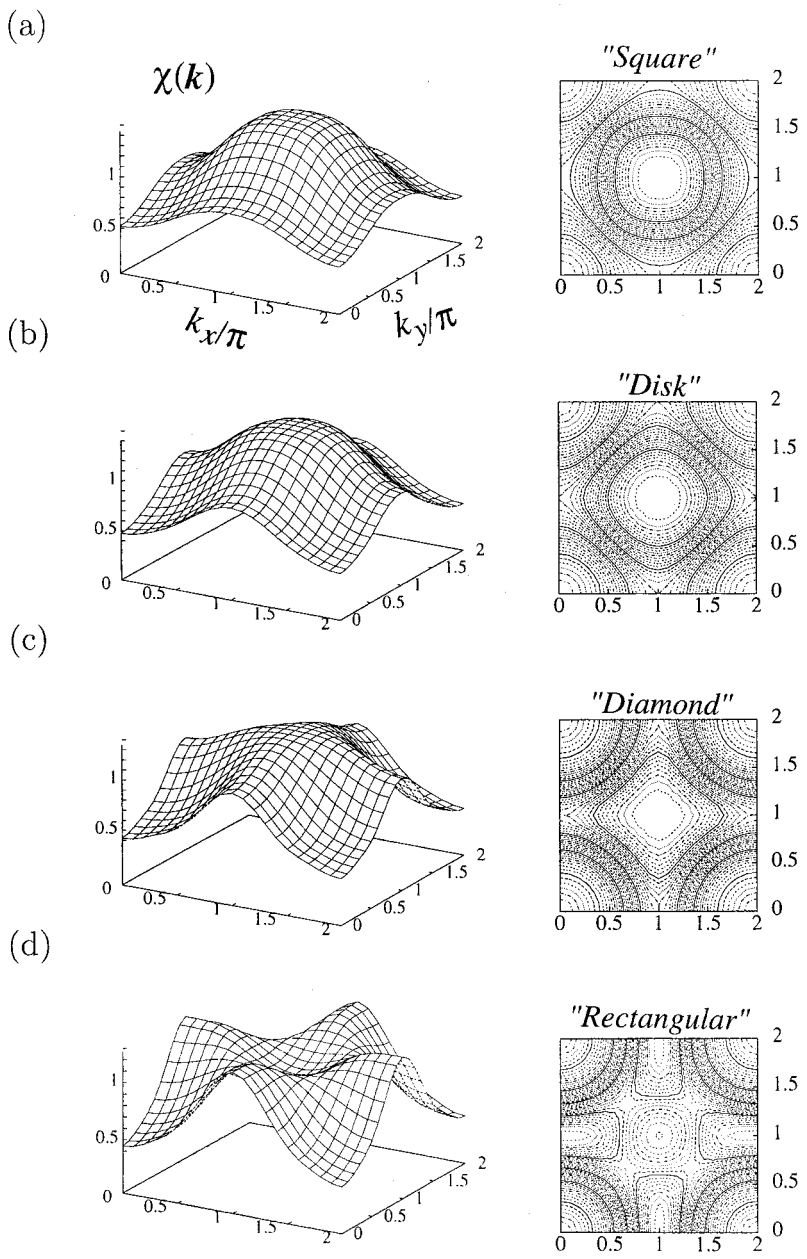


FIG. 4. The susceptibility $\chi(\boldsymbol{k})$ is plotted at $\tilde{T}=2.5$ along a line of $j_3=(1-2j_2)/4$ with appropriate parameters $(j_2,j_3)$: (a) (0.1,0.2), (b) (0.25,0.125), and (c) (0.4,0.05), respectively. In addition to the above cases, it is illustrated at the $C$-$H_1$ phase boundary with $j_2=0.75$ and $j_3=0.125$ at $\tilde{T}=3.0$. The relevant contour map is presented on the right-hand side.

mensurate paramagnetic phase incorporates suddenly with $\boldsymbol{k}_N^c$ (or $\boldsymbol{k}_C^c$) in the commensurate ones near the phase boundary, the effects of these modes amalgamate with each other and contribute to the susceptibility $\chi(\boldsymbol{k})$ almost equivalently. This leads to the appearance of the domain described above. Thus, one can say that the second-order phase transition occurs in this case via the intermediate phase bearing the domain structure. Depending on the locations of the relevant critical wave vectors, the domain presents rich shapes: it appears as square, disk, diamond, and rectangular, in the neighborhood of the $N$-$H_2$ phase boundary, the $H_1$-$H_2$-$N$ triple point, and the $N$-$H_1$ and $C$-$H_1$ phase boundaries, respectively.

For the neighborhood of the $N$-$H_1$-$C$ triple point, it demands a careful analysis because there are two different approaches to that point: one is provided by increasing $j_2$ to 0.5 with $j_3=0$ and the other is provided by decreasing $j_3$ to zero with $j_2=0.5$. Following the first route, one can see that the $N$ paramagnetic phase is stable for $j_2<0.45$, whereas the $C$ paramagnetic phase is stabilized for $j_2>0.55$. In the region $0.45\leqslant j_2\leqslant 0.55$, $\chi(\boldsymbol{k})$ hardly shows the wave-vector dependence along the $X$-$M$ direction regardless of the reduction of temperature. In particular, at $j_2=0.52$, it remains constant with its maximum value along that direction, while it peaks at the $M$ point along the $\Gamma$-$M$ direction in similar form, drawn in the inset of Fig. 5(a). This situation can be understood as follows: when the parameter $j_2$ is increased, the critical wave vector changes from $\boldsymbol{k}_N^c$ to $\boldsymbol{k}_C^c$ at the boundary $j_2=0.52$, where $\chi(\boldsymbol{k})$ keeps its maximum value at the $\boldsymbol{k}_N^c$ and $\boldsymbol{k}_C^c$ modes. Since these modes line up along $\overline{k_x}=\pm 1.0$ and $\overline{k_y}=\pm 1.0$, the formation of the cross-type domain is expected. In fact, the phase boundary shifts from $j_2=0.5$ denoted by the previous theory[5] as 0.52 because of the pre-

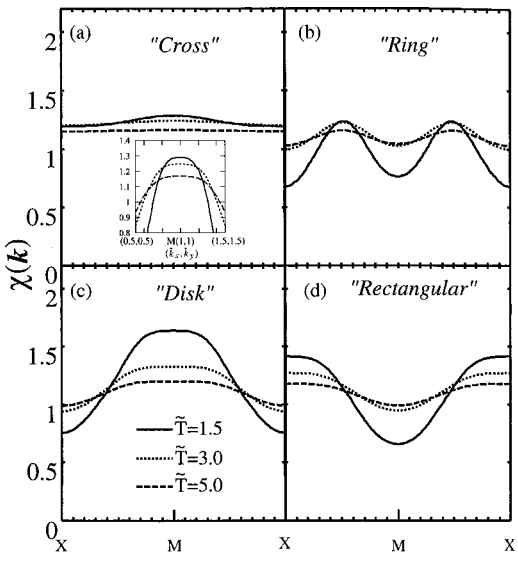


FIG. 5. The susceptibility $\chi(\boldsymbol{k})$ is presented at various temperature $\tilde{T}=1.5$, 3.0, and 5.0, along the $X$-$M$ direction for several intermediate phases called cross with $j_2=0.5$ and $j_3=0$ in (a), ring (0.5,0.25) in (b), disk (0.25,0.15) in (c), and rectangular (0.75,0.125) in (d). In the inset, the temperature dependence of $\chi(\boldsymbol{k})$ is plotted along $\Gamma$-$M$ direction for cross.

dominant effect of the Néel mode in the quantal case. Tracing the second route, the critical wave vector $\overline{\boldsymbol{k}^c_{H_1}}$ is fixed by constant $(\pm 0.5,1.0)$ or $(1.0,\pm 0.5)$, unless $j_3=0$. For $j_3>0.125$, $\boldsymbol{k}^p_{H_1}$ coincides with $\boldsymbol{k}^c_{H_1}$, so that the $H_1$ paramagnetic phase is stable; however, in the opposite case, $j_3<0.125$, $\boldsymbol{k}^p_{H_1}$ goes away from $\boldsymbol{k}^c_{H_1}$ and joins to $\boldsymbol{k}^c_N$ as $j_3\to 0$. Correspondingly, the $\boldsymbol{k}$ dependence of $\chi(\boldsymbol{k})$ is reduced along the $X$-$M$ direction, and approaches that of the cross-type domain. This is also interpreted in terms of the predominant effect of the Néel mode in the region for $j_3<0.125$, with $j_2=0.5$.

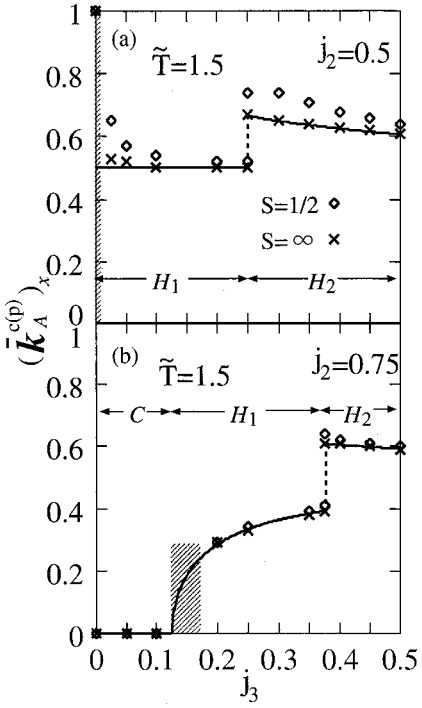


FIG. 6. The $x$ component of the peak position for susceptibility $\chi(\boldsymbol{k})$, $(k^p_A)_x$ is plotted versus various values of $j_3$ at $\tilde{T}=1.5$ with the symbol $\diamondsuit$ for $S=1/2$ and the symbol $\times$ for $S=\infty$: (a) $j_2=0.5$ and (b) $j_2=0.75$.

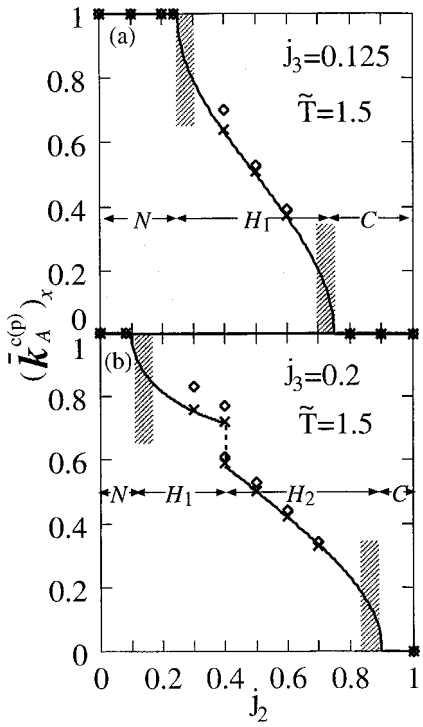


FIG. 7. The $x$ component of the peak position for susceptibility $\chi(\boldsymbol{k})$, $(k^p_A)_x$ is plotted versus various values of $j_2$ at $\tilde{T}=1.5$ with the symbol $\diamondsuit$ for $S=1/2$ and the symbol $\times$ for $S=\infty$: (a) $j_3=0.125$ and (b) $j_3=0.2$.

Finally, we draw up the domain map with the shaded area in Fig. 1 at $\tilde{T}=1.5$. It is interesting to note that this domain map is similar to the phase diagram[5] for $S=1/2$ in the ground state, except for the boundary between the $H_1$ and $H_2$ phases. Since the four magnetic configurations of the ordered phases and the local order patterns in the critical temperature region are specified commonly by the critical wave vector $\boldsymbol{k}^c_A$, we can suggest a possibility of the existence of the intermediated magnetic-disordered phase at $T=0$ around the domain region. And it seems to be closely connected with the spin liquid state, whether it is quantal or classical. Here, let us mention that it is found that the first-order phase transition occurs between the $H_1$ and $H_2$ phases from the analysis of the domain formation, so the intermediate phase or spin liquid state is not expected around this phase boundary.

## III. THE DYNAMICAL STRUCTURE FUNCTION

In the previous section, we have seen curious features of the static properties in the frustrated 2D $J_1$-$J_2$-$J_3$ model, and clarified that most of them are attributed to the competition among three kinds of antiferromagnetic couplings, $J_1$, $J_2$,

and $J_3$. In this section, we study how such competition affects the spin dynamics. The observed spectrum of inelastically scattered neutrons can be interpreted in terms of the dynamical spectrum function $F(\boldsymbol{k},\omega)$.[9] It is given by using the spin relaxation function $R(\boldsymbol{k},t)$ as

$$F(\boldsymbol{k},\omega)=\frac{1}{2\pi}\int_{-\infty}^{\infty}dt e^{i\omega t}\frac{R(\boldsymbol{k},t)}{R(\boldsymbol{k},0)},$$

$$=\frac{R(\boldsymbol{k},\omega)}{R(\boldsymbol{k},0)}, \tag{8}$$

where

$$R(\boldsymbol{k},t)=\int_0^{\beta}d\lambda\langle e^{\lambda H}S_k(0)e^{-\lambda H}S_{-k}(t)\rangle-\beta\langle S_k\rangle\langle S_{-k}\rangle. \tag{9}$$

If $R(\boldsymbol{k},t)$ is taken at $t=0$, it is proportional to the wave-vector-dependent susceptibility $\chi(\boldsymbol{k})$ as

$$\chi(\boldsymbol{k})=\frac{(g\mu_B)^2}{N}R(\boldsymbol{k},0). \tag{10}$$

Using the procedure introduced by Mori,[10] the Laplace transform of $F(\boldsymbol{k},\omega)$ is expanded into a continued fraction, i.e.,

$$\hat{F}(\boldsymbol{k},z)=\int_0^{\infty}dt e^{-zt}F(\boldsymbol{k},t)=\{z+\delta_1/[z+\delta_2/(z+\cdots)]\}^{-1}. \tag{11}$$

The coefficients $\delta_i$'s can be related to the reduced $m$th moments $\tilde{\Omega}_k^m$, which are the frequency moments of $F(\boldsymbol{k},\omega)$, defined by

$$\tilde{\Omega}_k^m=\int_{-\infty}^{\infty}d\omega\omega^m F(\boldsymbol{k},\omega)=\Omega_k^m/\Omega_k^0, \tag{12}$$

as

$$\delta_i=a_i/a_{i-1}, \tag{13}$$

with

$$a_0=1,$$

$$a_1=\tilde{\Omega}_k^2,$$

$$a_2=\tilde{\Omega}_k^4-(\tilde{\Omega}_k^2)^2,$$

$$a_3=\tilde{\Omega}_k^6-(\delta_1+\delta_2)\tilde{\Omega}_k^4,$$

$$\vdots.$$

In Eq. (12) $\Omega_k^m$ is the $m$th frequency moment of $R(\boldsymbol{k},\omega)$ and given by

$$\Omega_k^m=\int_{-\infty}^{\infty}d\omega\omega^m R(\boldsymbol{k},\omega) \tag{14}$$

$$=\beta^{-1}\sum_{lj}\exp\{i\boldsymbol{k}\cdot(\boldsymbol{l}-\boldsymbol{j})\}\left(\frac{i}{\hbar}\right)\times\left\langle\left[S_l(0),\frac{\partial S_j(t)^{m-1}}{\partial t^{m-1}}\right]\right\rangle\Bigg|_{t=0}. \tag{15}$$

The reduced $m$th moment is calculated by means of the high-temperature series expansion, and expressed as

$$\tilde{\Omega}_k^m=[1/J_1]\sum_{n=0}^{\infty}W_{mn}(j_2,j_3;\boldsymbol{k})\Theta^{-n}. \tag{16}$$

By symmetry, all the odd moments $\tilde{\Omega}_k^{2m+1}(m>0)$ vanish. The calculated coefficients $W_{mn}(j_2,j_3;\boldsymbol{k})$ are tabulated[14] at two points $M$ and $X$, for $m=2$, with $0\leqslant n\leqslant 5$, for $m=4$, with $0\leqslant n\leqslant 3$, and for $m=6$, with $0\leqslant n\leqslant 1$, by putting $S=1/2$ and $J_1=1$.

Following the approximation of a Gaussian termination[17] for the continued fraction at the third level, we get

$$\hat{F}(\boldsymbol{k},i\omega)=\cfrac{1}{i\omega+\cfrac{\delta_1}{i\omega+\delta_2 f_2\left(\cfrac{\omega}{\delta_3^{1/2}}\right)}}, \tag{17}$$

where

$$f_2(x)=\delta_3^{-1/2}e^{-x^2/2}\left[\left(\frac{1}{2}\pi\right)^{1/2}-i\int_0^x dy e^{y^2/2}\right]. \tag{18}$$

As a result, we can evaluate $F(\boldsymbol{k},\omega)$ directly from the relationship

$$F(\boldsymbol{k},\omega)=\pi^{-1}\mathrm{Re}\,\hat{F}(\boldsymbol{k},i\omega). \tag{19}$$

### A. Four stable paramagnetic cases

As a first step, let us examine the transfer wave vector and the frequency dependence of the dynamical spectrum function $F(\boldsymbol{k},\omega)$ for four stable $N$, $C$, $H_1$, and $H_2$ paramagnetic phases. At small wave vector $\boldsymbol{k}\simeq 0$, $F(\boldsymbol{k},\omega)$ exhibits a Lorentzian due to the spin diffusion process, and the sharp peak of $F(\boldsymbol{k},\omega)$ is expected at $\omega=0$ and $\boldsymbol{k}=0$, which indicates the total spin conservation. For the other cases, however, $F(\boldsymbol{k},\omega)$ shows various structures depending on $\boldsymbol{k}$.

At the high-temperature limit, with an increasing $\boldsymbol{k}$ value, a broad shoulder appears in $F(\boldsymbol{k},\omega)$ with width $\omega_{sh}$. Furthermore, for some cases, this shoulder turns into a hump situated at finite frequency $\omega_J$ as $\boldsymbol{k}$ approaches to $\boldsymbol{k}_A^c$. In Figs. 8(a)–8(d), $F(\boldsymbol{k}_A^c,\omega)$ is plotted versus the reduced frequency $\bar{\omega}(=\omega/J_1)$ for the same parameters $(j_2,j_3)$ as those in Figs. 2(a)–2(d), respectively. The $\boldsymbol{k}$ dependence of the shoulder width $\bar{\omega}_{sh}$ or $\bar{\omega}_J$ is illustrated for each case in Figs. 9(a)–

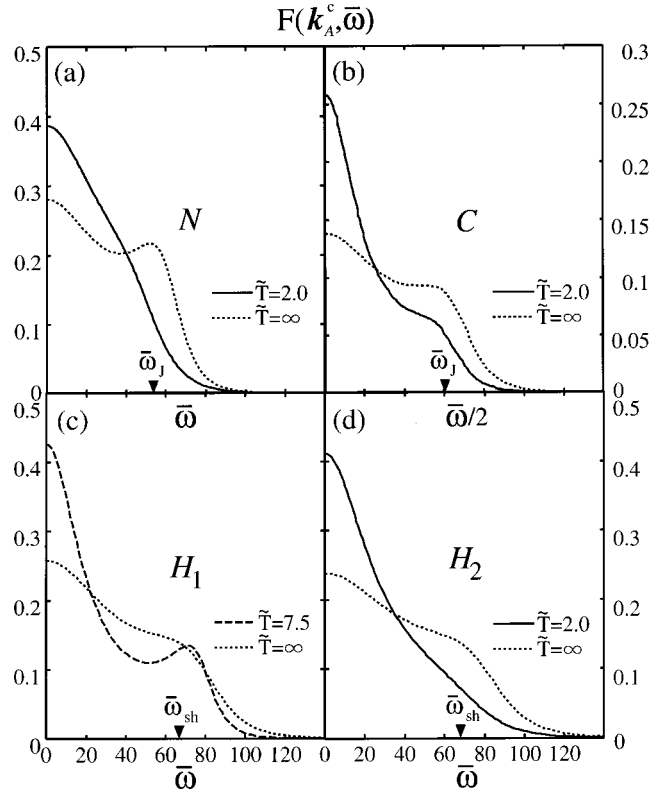


FIG. 8. The dynamical spectrum function $F(\boldsymbol{k}_A^c,\omega)$ is plotted versus the reduced frequency $\bar{\omega}(=\omega/J_1)$ at $\tilde{T}=\infty$ and 2.0 for (a) $A=N$, (b) $A=C$, and (d) $A=H_2$ paramagnetic phase. For the $H_1$ paramagnetic phase $F(\boldsymbol{k}_A^c,\omega)$ is given in (c) at $\tilde{T}=\infty$ and 7.5.

9(d), and compared with the corresponding square root of the reduced second moment $\sqrt{\tilde{\Omega}_k^2}$, which is given at $T=\infty$ in following simple form:

$$\sqrt{\tilde{\Omega}_k^2}/(2J_1)=[\{2-\cos(k_x)-\cos(k_y)\} + j_2^2\{2-\cos(k_x+k_y)-\cos(k_x-k_y)\} + j_3^2\{2-\cos(2k_x)-\cos(2k_y)\}]^{1/2}. \quad (20)$$

Roughly speaking, their $\boldsymbol{k}$ dependences coincide with each other. From the expression of Eq. (20), it is considered that the appearance of a shoulder or hump (damped side peak) in $F(\boldsymbol{k}_A^c,\bar{\omega})$ is responsible for the spin flip-flop motions governed by the critical wave vector $\boldsymbol{k}_A^c$.[17] In fact, the local spin flip-flop motions occur rapidly between first, second, and third neighbors at high temperature, so the side peak, etc., is barely seen in $F(\boldsymbol{k},\bar{\omega})$ due to the strong motional narrowing. However, when the transfer wave vector of incident neutrons, for instance, approaches $\boldsymbol{k}_A^c$, it is resonant with the characteristic spin flip-flop motion at $\omega\sim\omega_J$ (or $\omega_{sh}$). This should create the form of the damped side peak or shoulder in the response function. In other words, one can specify $\boldsymbol{k}_A^c$ by the measurement of the peak position $\omega_J$ or shoulder width $\omega_{sh}$ in the inelastic neutron scattering cross section, even if there is at high-temperature limit.

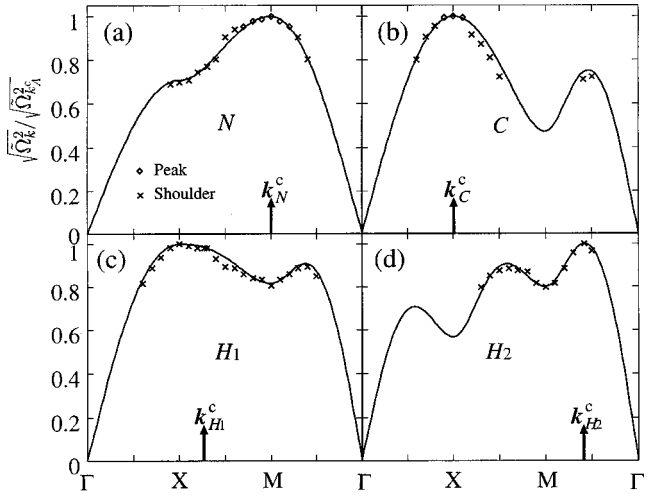


FIG. 9. The $\boldsymbol{k}$ dependence of the side peak position $\omega_J$ (shoulder width $\omega_{sh}$) is plotted with a symbol $\diamond$ ($\times$) at $T=\infty$, corresponding to Fig. 8 for (a) $N$, (b) $C$, (c) $H_1$, and (d) $H_2$. The related square root of the reduced second moment $\sqrt{\tilde{\Omega}_k^2}$ is illustrated as a function of $\boldsymbol{k}$. Each quantity is normalized by its maximum value.

The present series expansions for the frequency moments $\tilde{\Omega}_k^m$ ($m=0$, 2, 4, and 6) are too short to discuss for the spin dynamics in the low-temperature region; however, it is expected to extract some precursor about it from investigation of $F(\boldsymbol{k},\bar{\omega})$ at the finite temperature. On account of the convergence for such series expansion, the temperature is limited for meaningful discussion to $\tilde{T}\geqslant 2.0$ for $N$, $C$, and $H_2$, and $\tilde{T}\geqslant 7.5$ for $H_1$ paramagnetic phases. In Figs. 8(a)–8(d), $F(\boldsymbol{k}_A^c,\omega)$ is presented at the approvable lowest temperature for each case.

The effect of the temperature reduction on spin dynamics is definitely found, i.e., the line shape becomes considerably narrowed. To understand this situation, the investigation of the half-width of $F(\boldsymbol{k},\omega)$, $\Delta\omega_H(\boldsymbol{k})$ is useful. For instance, $\Delta\omega_H(\boldsymbol{k})$ are displayed in Figs. 10(a) and 10(b) for the $N$ and $H_1$ paramagnetic phases at $\tilde{T}=2.0$, and compared with the corresponding second moment and the spin-wave excitation $\omega(\boldsymbol{k})_{sp}$ for various $\boldsymbol{k}$ values. Here, let us remark on the linear spin-wave dispersion relation:[16]

$$\omega(\boldsymbol{k})_{sp}=2J_1S\sqrt{s_{\boldsymbol{k}}d_{\boldsymbol{k}}}, \quad (21)$$

with

$$s_{\boldsymbol{k}}=\sum_{i=1}^{3} j_i \sum_{\boldsymbol{\delta}_i} (\cos\boldsymbol{k}_A^c\cdot\boldsymbol{\delta}_i-\cos\boldsymbol{k}\cdot\boldsymbol{\delta}_i), \quad (22a)$$

$$d_{\boldsymbol{k}}=\sum_{i=1}^{3} j_i \sum_{\boldsymbol{\delta}_i} \cos\boldsymbol{k}_A^c\cdot\boldsymbol{\delta}_i(1-\cos\boldsymbol{k}\cdot\boldsymbol{\delta}_i), \quad (22b)$$

where $\boldsymbol{\delta}_i$ is a vector joining a site with the $i$th nearest neighbors. Equation (21) denotes that there are two kinds of soft modes, the $\boldsymbol{k}=0$ and $\boldsymbol{k}=\boldsymbol{k}_A^c$, which are consequences of the kinematical slowing down and Goldstone theorem. Interestingly, in the vicinity of $\boldsymbol{k}_A^c$, the wave-vector dependence of

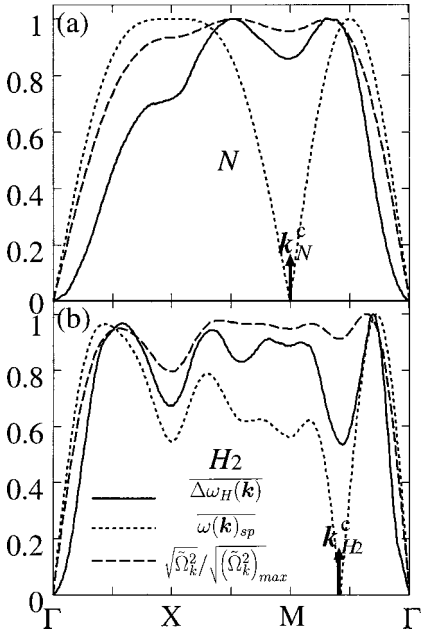


FIG. 10. The half-width $\overline{\Delta\omega_H(\boldsymbol{k})}$ (solid line) is compared with the spin-wave excitation $\overline{\omega(\boldsymbol{k})_{sp}}$ (dotted line) described in Eq. (21) and the square root second moment $\sqrt{\tilde{\Omega}_k^2}/(\sqrt{\tilde{\Omega}_k^2})_{max}$ (broken line) for various $\boldsymbol{k}$ values, for (a) the $N$ paramagnetic phase, with $j_2=j_3=0$ and (b) the $H_2$ paramagnetic phase with $j_2=0$ and $J_3=1.0$. Here, $\overline{A}$ means the normalization by $A_{max}$, i.e., $\overline{A}=A/A_{max}$.

$\Delta\omega_H(\boldsymbol{k})$ and the second moment are completely opposite to that at the high-temperature limit. They seem to be like the profile of the spin-wave dispersion $\omega(\boldsymbol{k})_{sp}$, because it forms a hollow as $\boldsymbol{k}\rightarrow\boldsymbol{k}_A^c$, although it remains finite at $\boldsymbol{k}=\boldsymbol{k}_A^c$. This can be explained in terms of the short-range magnetic order developed at a finite temperature.[18,19] As the temperature is lowered, the correlation appears among the local situations, so a certain kind of short-range magnetic order must be developed with temperature-dependent finite size $\xi(T)$ and finite lifetime $\tau(T)$. Since the spin arrangement is considerably ordered at least inside this short-range order, the modes with large enough $\boldsymbol{k}$, i.e., $\boldsymbol{k}\xi>1$, behave very much like spin waves for a while, approximately during $\tau$. This spin-wave-like mode is usually called a ''sloppy spin wave.''[18,19] These circumstances are reflected in the same spectrum as over damped spin wave modes situated at $\omega\sim\omega_{sp}(\boldsymbol{k})$. In contract to this, for the modes with small enough $\boldsymbol{k}$, i.e., $\boldsymbol{k}\xi<1$, one cannot expect any oscillatory collective excitation, but the diffusive behavior in spin propagation, and the spectrum leads to a slight hump with maximum at $\omega=0$. At the considered temperature $\tilde{T}=2.0$, there exist so many kinds of magnetic short-range orders in several size $\xi$ and lifetime $\tau$ that both behaviors, i.e, the quasi-spin-wave modes and the diffusive modes, are observed in the spectrum $F(\boldsymbol{k},\omega)$.

### B. Intermediate phases

We now turn to a discussion on the dynamics in the intermediate phases. In a way similar to the stable paramagnetic phases, the shoulder appears dependent on $\boldsymbol{k}$ at $T=\infty$. In Figs. 11(a) and 11(b), $\omega(\boldsymbol{k})_{sh}$ is plotted as a function $\boldsymbol{k}$ for the cross and ring cases. The corresponding second moment is also plotted. In comparison with the typical stable four cases, the $\boldsymbol{k}$ variation appears rather sluggish, except for the drastic narrowing around $\boldsymbol{k}\rightarrow 0$. This is due to the fact that no unique specified critical wave vector exists in these cases, but several $\boldsymbol{k}$'s indicated by arrows in Figs. 11(a) and 11(b) can contribute dominantly to $F(\boldsymbol{k},\overline{\omega})$ [see Eq. (20)].

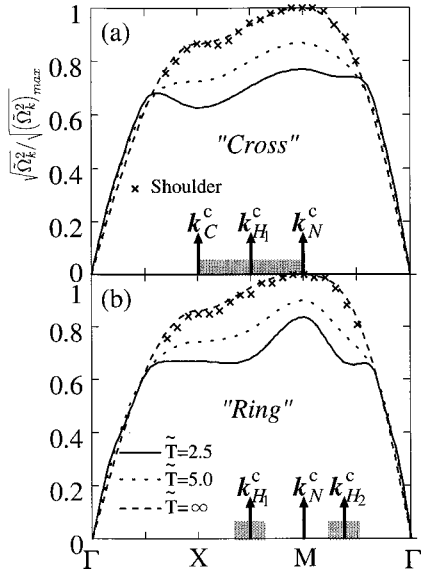


FIG. 11. The $\boldsymbol{k}$ dependence of shoulder width $\omega_{sh}/(\omega_{sh})_{max}$ is plotted with the symbol $\times$ at $T=\infty$ for two intermediate phase: (a) cross, with $j_2=0.5$ and $j_3=0$ and (b) ring with $j_2=0.5$ and $j_3=0.25$. The related square root of the second moment $\sqrt{\tilde{\Omega}_k^2}/(\sqrt{\tilde{\Omega}_k^2})_{max}$ is plotted at $\tilde{T}=\infty$ (broken), $\tilde{T}=5.0$ (dotted), and $\tilde{T}=2.5$ (solid line). Each quantity is normalized by its maximum value.

At a finite temperature, the situations are less clear due to the limited length of the series for the frequency moments. However, some dynamical features are captured by the analysis of the $\boldsymbol{k}$ dependence of the second frequency moment $\tilde{\Omega}_k^2$. The corresponding reduced second moment is added in Fig. 11 at $\tilde{T}=5.0$ and 2.5. In contrast to the remarkable temperature dependence in the stable paramagnetic phases, each $\boldsymbol{k}$ dependence changes slightly with a decrease in the temperature, especially over domain (shaded parts in Fig. 11), and keeps the high-temperature dynamical aspect, in a sense that a broad maximum stays around the $M$ point. This is interpreted that the collective propagationlike mode is not expected in these cases due to the frustration effect, and the spin-flop motion driven by the dominant Néel mode survives although the temperature is decreased.

## IV. SUMMARY

By using the high-temperature series expansion method, static and dynamical properties are investigated for the 2D square quantum Heisenberg antiferromagnets with competing interactions up to third neighbors ($J_1$-$J_2$-$J_3$ model).

The wave-vector-dependent susceptibility $\chi(\boldsymbol{k})$ is calculated up to the seventh order of $\Theta$. Although our series are not sufficient to give the critical discussion in the low-temperature region, the convergence of the series seems to give us reasonable results for $\tilde{T} \geqslant 2.0$ ($\tilde{T} \geqslant 1.5$ for some static properties). Thus we can expect to extract some precursor of the peculiarities in the low temperature by analysis of $\chi(\boldsymbol{k})$ around the critical temperature region $\tilde{T} \cong 2.0$ or so.

We find four kinds of stable paramagnetic phases: Néel, collinear, and two helical $H_1$ and $H_2$ ones in the proper range of the $J_1$-$J_2$-$J_3$ space. They are characterized by the critical wave vector $\boldsymbol{k}_A^c$ ($A=N$, $C$, $H_1$, or $H_2$), at which the functions $\chi(\boldsymbol{k})$ show their maximum values.

Interestingly, this $\boldsymbol{k}_A^c$ coincides with the wave vector that specifies the spin configuration in the ordered state. This means that there is a similarity between the highly developed magnetic short-range order and the long-range order. Except around the $H_1$-$H_2$ phase boundary, the four stable typical paramagnetic phases are destabilized; instead, the intermediate phases appear in the neighborhood of the corresponding phase boundary. In the intermediate phase, it remains constant with its maximum value spread over a certain range on the ($k_x$-$k_y$) plane, which is referred to here as a domain. It is verified that the frustration effects, attributed to the competing interactions $J_i$ ($i=1,2,3$), are indispensable for such domain formation, and the shape varies depending on the kind of frustration it is concerned with, whether it is quantal or classical. The analogy between the paramagnetic phase diagram obtained here and the ordered one derived by the simple spin-wave theory suggests the possibility that the intermediate phases turn into the spin liquid state as $T \to 0$. However, such a state is not anticipated around the $H_1$-$H_2$ phase transition, because it is the first-order phase transition.

The dynamical spectrum function $F(\boldsymbol{k},\omega)$ is evaluated in the form of Mori's continued fraction by using the approximation of a Gaussian termination at the third level. Here, the coefficients $W_{mn}(j_2,j_3;\boldsymbol{k})$ defined in Eq. (16), are calculated up to the fifth, third, and first orders of $\Theta$ for $m=2$, 4, and 6, respectively.

For arbitrary cases, $F(\boldsymbol{k},\omega)$ shows a sharp peak at $\omega=0$ and $\boldsymbol{k}=0$, regardless of the temperature, due to the kinematical slowing down. The dynamical behavior for the four stable paramagnetic phases is also characterized by the critical wave vector $\boldsymbol{k}_A^c$: at $T=\infty$, the side peak or shoulder shape appears at $\boldsymbol{k} \simeq \boldsymbol{k}_A^c$, due to the local flip-flop motion, and the line shape becomes considerably narrow as the temperature decreases due to the quasicollective motion. In the intermediate phase, the line shape at $T=\infty$ undergoes a slow change versus the wave vector $\boldsymbol{k}$ except for the drastic narrowing around $\boldsymbol{k} \simeq 0$. This is due to the absence of the unique critical wave vector, and several $\boldsymbol{k}$'s contribute to $F(\boldsymbol{k},\omega)$ almost equivalently. It is known from the analysis of the second frequency moments that the high-temperature dynamical aspect is retained even if the temperature is decreased, due to the frustration effect.

## ACKNOWLEDGMENTS

One of the authors (K.K.) is very grateful to Professor R.A. Tahir-Kheli of Temple University for helpful discussions in the early stage of this work. We are indebted to Professor S. Iwabuchi for his valuable contributions.

*Present address: System Integration Technology Center, Toshiba Corp., 3-22 Katamachi, Fuchu, Tokyo 183-8512, Japan.

[1] T. Nakamura and N. Hatano, J. Phys. Soc. Jpn. **62**, 3062 (1993).

[2] J. E. Hirsch and S. Tang, Phys. Rev. B **39**, 2887 (1989); M. P. Gelfand, R. R. P. Singh, and D. A. Huse, *ibid.* **40**, 10 801 (1989); T. Oguchi and H. Kitatani, J. Phys. Soc. Jpn. **59**, 3322 (1990); J. Igarashi, *ibid.* **62**, 4449 (1993); R. R. P. Singh, Z. Weihong, C. J. Hamer, and J. Oitmaa, Phys. Rev. B **60**, 7278 (1999).

[3] J. H. Xu and C. S. Ting, Phys. Rev. B **42**, 6861 (1990); H. Nishimori and Y. Saika, J. Phys. Soc. Jpn. **59**, 4454 (1990).

[4] P. Chandra and B. Doucot, Phys. Rev. B **38**, 9335 (1988); A. Chubukov, *ibid.* **44**, 392 (1991); E. Rastelli and A. Tassi, *ibid.* **46**, 10 793 (1992); J. Ferrer, *ibid.* **47**, 8769 (1993).

[5] A. Moreo, E. Dagotto, T. Jolicoeur, and J. Riera, Phys. Rev. B **42**, 6283 (1990).

[6] J. G. Bednorz and K. A. Müller, Z. Phys. B: Condens. Matter **64**, 189 (1986).

[7] H. J. Schulz, T. A. L. Ziman, and D. Poilblanc, in *Magnetic Systems with Competing Interactions*, edited by H. T. Diep (World Scientific, Singapore, 1994), Chap. 3, p. 127, and references cited therein.

[8] S. Doniach, M. Inui, V. Kalmeyer, and M. Gabay, Europhys. Lett. **6**, 633 (1988).

[9] W. Marshall and S. W. Lovesey, *Theory of Thermal Neutron Scattering* (Clarendon Press, Oxford, 1971).

[10] H. Mori, Prog. Theor. Phys. **33**, 423 (1965); **34**, 399 (1965).

[11] K. Kawasaki and R.A. Tahir-Kheli, Phys. Rev. B **15**, 2741 (1977); **17**, 2245 (1978).

[12] K. Kawasaki, K. Tanaka, C. Hamamura, and R. A. Tahir-Kheli, Phys. Rev. B **45**, 5321 (1992).

[13] G. S. Rushbrooke, G. A. Baker, Jr., and P. J. Wood, in *Phase Transitions and Critical Phenomena*, edited by C. Domb and M. S. Green (Academic, New York, 1974), Vol. 3, Chap. 5, p. 294, and references cited therein.

[14] S. Kurata, Doctoral thesis, Nara Women's University, Nara, 2000.

[15] N. D. Mermin and H. Wagner, Phys. Rev. Lett. **17**, 1133 (1966).

[16] U. Balucani and E. Rastelli, in *Magnetic Properties of Matter*, edited by F. Borsa and V. Tognetti (World Scientific, Singapore, 1986), Chap. 2, and references cited therein.

[17] K. Kawasaki, N. Miyamoto, and R. A. Tahir-Kheli, J. Phys. C **15**, 2735 (1982).

[18] H. Tomita and H. Mashiyama, Prog. Theor. Phys. **48**, 1133 (1972).

[19] K. Tomita and K. Kawasaki, Prog. Theor. Phys. **49**, 1858 (1973); Y.-J. Wang, M.-R. Li, and C.-D. Gong, Phys. Rev. B **56**, 10 982 (1997).